This article has been accepted for inclusion in a future issue of this journal. Content is final as presented, with the exception of pagination.

Robust and Collision-Free Formation Control of Multiagent Systems With Limited Information

Yang Fei, Peng Shi, *Fellow, IEEE*, and Cheng-Chew Lim, *Life Senior Member, IEEE*

***Abstract*— This article investigates the collision-free cooperative formation control problem for second-order multiagent systems with unknown velocity, dynamics uncertainties, and limited reference information. An observer-based sliding mode control law is proposed to ensure both the convergence of the system's tracking error and the boundedness of the relative distance between each pair of agents. First, two new finite-time neural-based observer designs are introduced to estimate both the agent velocity and the system uncertainty. The sliding mode differentiator is then employed for every agent to approximate the unknown derivatives of the formation reference to further construct the limited-information-based sliding mode controller. To ensure that the system is collision-free, artificial potential fields are introduced along with a time-varying topology. An example of a multiple omnidirectional robot system is used to conduct numerical simulations, and necessary comparisons are made to justify the effectiveness of the proposed limited-information-based control scheme.**

***Index Terms*— Collision avoidance, formation control, multiagent systems, neural-based observer, sliding mode control.**

I. Introduction

IN RECENT decades, multiagent systems' cooperative control problems [1]–[4] have been highly attractive due to their applications in areas such as distributed sensor networks [5] and robotic systems [6]. Among the numerous specific disciplines of cooperative control, the distributed formation control issue [7]–[9] is widely investigated to provide algorithms to control real-time platforms, such as ground rovers [10] to complete practical tasks.

Various robust control methods have been proposed to ensure system stability when uncertainty exists. A Q-learning-based approach was proposed in [11] to perform optimal robust control for nonlinear systems. In [12], an observer-based H_∞ approach was presented for a class of quantized networked control systems to ensure robustness with the existence of randomly occurring uncertainties. For second-order systems, sliding mode control [13]–[15] is one popular method to achieve fast error convergence and maintain system robustness.

Manuscript received December 18, 2020; revised June 5, 2021 and August 28, 2021; accepted September 8, 2021. This work was supported in part by Australian Research Council under Grant DP170102644. *(Corresponding author: Peng Shi.)*

The authors are with the School of Electrical and Electronic Engineering, The University of Adelaide, Adelaide, SA 5005, Australia (e-mail: y.fei@adelaide.edu.au; peng.shi@adelaide.edu.au; cheng.lim@adelaide.edu.au).

Color versions of one or more figures in this article are available at https://doi.org/10.1109/TNNLS.2021.3112679.

Digital Object Identifier 10.1109/TNNLS.2021.3112679

The global sliding mode scheme was used along with a recurrent neural network in [15] to perform adaptive control for dynamic systems. An adaptive dynamic sliding mode control scheme was proposed in [13] to regulate system formations. However, most results are inapplicable if either system states or state references are not completely known, leading to a lack of robustness. Hence, how to perform sliding mode control with limited information in both system states and their references becomes one big gap to fill.

For practical systems with restricted sensing capabilities, observers [16], [17] are usually employed to estimate the inaccessible system states. Extended state observer was used in [16] to approximate the uncertainties of followers and the unknown control input of the leader for the formation tracking of high-order multiagent systems. A type of observer was constructed for rigid spacecraft to achieve finite-time convergence of the estimation error [17]. However, observers with similar structures are only capable to approximate energy-bounded uncertainties, and the high gain design is hard to realize for practical implementations.

To face the aforementioned issues, the idea of a neural-based observer was first brought up in [18], where a dynamic recurrent neural-based observer was developed. Radial basis function neural networks (RBFNNs) were used in [19] to build up adaptive observers to perform backstepping control. Currently, one unsolved challenge for the neural-based observer is that no existing design can guarantee finite-time characteristics.

With part of the necessary system information being unknown, there is a high chance that agents will collide with each other before the control input is stabilized. Therefore, collision avoidance techniques are essential to ensure the safety of every agent. For ideal and completely known systems, the dynamic window approach [20] is commonly used to generate smooth and optimal trajectories for robots. However, motion control approaches, such as artificial potential field (APF) [9], are more suitable for systems with uncertainties.

A collision-free consensus algorithm was proposed in [21] for autonomous underwater vehicles with static communication topology. The problem of connectivity assurance was further considered along with the collision avoidance issue for a group of mobile robots in [9]. However, such results are far from satisfactory because potential collisions are still expected for agent pairs without direct communication if the system topology is assumed to be static. Hence, how to ensure that every agent pair is collision-free becomes an important issue.

Motivated by the above challenges, this article focuses on the robust and collision-free formation control problems for a group of second-order agents with limited information. The contributions of this article are listed as follows.

1) Instead of having a static system topology, such as [9], a range-based topology is constructed to ensure the effectiveness of the collision avoidance scheme.
2) On the basis of [19], the finite-time theory is first achieved in a neural-based observer. A new error-related parameter design is further employed to attenuate chattering and increase estimation accuracy.
3) Compared with [10], a new limited-information-based sliding mode formation controller is designed to guarantee the boundedness of tracking error without knowing the agent velocity and the speed reference.

This article has been organized as follows. The dynamics of the multiagent system, the modeling of the communication graph, and the knowledge of RBFNN and APF are given in Section II. The design of finite-time neural-based state observer and the limited-information-based sliding mode controller is presented in Section III. Numerical simulations and their results are illustrated in Section IV, while Section V contains our final conclusions of this article.

Notations: Throughout this article, let $\otimes$ represent the Kronecker production and I_n denote an identity matrix with the dimension of n. Apart from that, we have $\mathrm{sgn}^{\beta}(\mathbf{o}) = \mathrm{diag}\{\mathrm{sign}(\mathbf{o})\}[|o_1|^{\beta}, |o_2|^{\beta}, \ldots, |o_n|^{\beta}]^{\mathrm{T}}$, where $\beta \in \mathbb{R}$ and $\mathbf{o} = [o_1, o_2, \ldots, o_n]^{\mathrm{T}}$, for simplicity. For a matrix $\mathcal{M}$, the term $\|\mathcal{M}\|_F$ represents its Frobenius norm. If $\mathcal{M}$ is a square matrix, we have $\overline{\sigma}(\mathcal{M})$ and $\underline{\sigma}(\mathcal{M})$ as the maximum and minimal eigenvalues of $\mathcal{M}$, respectively.

II. Preliminaries

A. System Model

Consider a group of nonlinear agents with second-order dynamics that are written as

$$\begin{cases} \dot{x}_i = \upsilon_i \\ \dot{\upsilon}_i = f_i + g_i u_i + \bar{\omega}_i, \quad i = 1, 2, \ldots, N \end{cases} \tag{1}$$

where $x_i = [x_{pi}^{\mathrm{T}}, x_{\theta i}^{\mathrm{T}}]^{\mathrm{T}} \in \mathbb{R}^n$ is the observable position information, $\upsilon_i = [\upsilon_{pi}^{\mathrm{T}}, \upsilon_{\theta i}^{\mathrm{T}}]^{\mathrm{T}} \in \mathbb{R}^n$ is the inaccessible velocity information, $x_{pi}, \upsilon_{pi} \in \mathbb{R}^{n_1}$ are the agent's linear states, $x_{\theta i}, \upsilon_{\theta i} \in \mathbb{R}^{n_2}$ are the agent's angular states, $f_i \in \mathbb{R}^n$ is the unknown system dynamics, $\bar{\omega}_i \in \mathbb{R}^n$ is the external disturbance, $g_i \in \mathbb{R}^{n\times n}$ is the known nonlinear control gain matrix, and $u_i \in \mathbb{R}^n$ represents the control input. The aforementioned parameters satisfy the conditions that $n_1 \geq 2$, $n_2 \geq 0$, and $n_1 + n_2 = n$. If we have $\omega_i = f_i + \bar{\omega}_i$ to represent the overall uncertainty, we rewrite (1) as

$$\begin{cases} \dot{x}_i = \upsilon_i \\ \dot{\upsilon}_i = g_i u_i + \omega_i, \quad i = 1, 2, \ldots, N. \end{cases} \tag{2}$$

Define $x = [x_1^{\mathrm{T}}, x_2^{\mathrm{T}}, \ldots, x_N^{\mathrm{T}}]^{\mathrm{T}}$, $\upsilon = [\upsilon_1^{\mathrm{T}}, \upsilon_2^{\mathrm{T}}, \ldots, \upsilon_N^{\mathrm{T}}]^{\mathrm{T}}$, $\omega = [\omega_1^{\mathrm{T}}, \omega_2^{\mathrm{T}}, \ldots, \omega_N^{\mathrm{T}}]^{\mathrm{T}}$, and $g = \mathrm{diag}\{g_1, g_2, \ldots, g_N\}$; we are then able to obtain the cluster's dynamics as

$$\begin{cases} \dot{x} = \upsilon \\ \dot{\upsilon} = gu + \omega. \end{cases} \tag{3}$$

Definition 1 ([10]): For a state vector $\mathcal{X} \in \mathbb{R}^n$, if there exists a compact set $\Omega_{\mathcal{X}} \in \mathbb{R}^n$, a positive number $b_{\mathcal{X}}$, and a time $t_{\mathcal{X}}(\mathcal{X}(t_0), b_{\mathcal{X}})$ such that, for all $\mathcal{X}(t_0) \in \Omega_{\mathcal{X}}$, the equation $\|\mathcal{X}\| \leq b_{\mathcal{X}}$ is guaranteed when $t \geq t_0 + t_{\mathcal{X}}$, then the state $\mathcal{X}$ is said to be uniformly ultimately bounded (UUB).

Lemma 1 ([10]): For a positive definite function $V(\mathcal{X})$, if there is a positive boundary $b_{\mathcal{X}}$ such that $\dot{V}(\mathcal{X})$ is expected to remain negative when $\|\mathcal{X}\| > b_{\mathcal{X}}$, then the uniform ultimate boundedness of the state $\mathcal{X}$ is guaranteed.

The position reference for the ith agent is illustrated as $x_{di} \in \mathbb{R}^n$ $(i = 1, 2, \ldots, N)$. The aim of this article is to achieve the uniform ultimate boundedness of each agent's position tracking error, which is specified as

$$\lim_{t\to\infty} ||x_i(t) - x_{di}(t)|| \leq \mu, \quad i = 1, 2, \ldots, N \tag{4}$$

where μ is a small positive constant. The following assumptions are made on the basis of the unified model (1):

Assumption 1: The system states x_i and υ_i, and the unknown function ω_i are all bounded.

Assumption 2: The ith agent can get access to the position reference. The norm $\|x_{di} - x_{dj}\| (j \in [1, N])$ remains bounded. Furthermore, x_{di} is at least second-order differentiable, but its time derivatives are not directly provided to the agent. The variable $\ddot{x}_{di}$ has a Lipschitz constant $\beta_{i,x}$.

B. Graph Theory

In this design, the communication topology of the multiagent system is described by a weighted directed graph $G = \{R(G), E(G), A(G)\}$, where $R(G) = \{r_1, r_2, \ldots, r_N\}$ is the set of nodes, $E(G) \subseteq R \times R$ represents the set of edges, and $A(G) = [a_{ij}] \in \mathbb{R}^{N\times N}$ is the adjacency matrix with nonnegative elements. The overall communication graph G consists of two subgraphs G_1 and G_2 that satisfy $A(G) = A_1 + A_2$, where A_k $(k = 1, 2)$ is the adjacency matrix for graph G_k. G_1 is a static directed graph that represents the distance-invariant communication topology, and G_2 is a time-varying graph that illustrates the information exchange achieved by limited range communication approaches.

We use terms a_{ji}^k and e_{ji}^k to represent the element in the jth row and the ith column of matrix A_k, and the directed edge from r_j to r_i in graph G_k for $i, j \in [1, N]$, respectively. We consider $a_{ii}^k = 0$ for both subgraphs. In graph G_k, node r_j is considered as the neighbor of r_i if and only if the directed edge e_{ji}^k exists. The element a_{ji}^1 satisfies $a_{ji}^1 = 1$ if and only if the edge e_{ij}^1 exists. In G_2, the edge e_{ij}^2 is built when the relative distance between the node pair (r_i, r_j) is not larger than R_c if and only if e_{ij}^1 does not exist, which leads to

$$a_{ji}^2 = \begin{cases} f\left(\|z_{ij}\|\right), & \|z_{ij}\| \leq R_c \;\; a_{ji}^1 = 0 \;\text{ and } i \neq j \\ 0, & \text{otherwise} \end{cases} \tag{5}$$

where $z_{ij} = x_{pi} - x_{pj}$, $R_c \in \mathbb{R}^+$, and $f(\|z_{ij}\|)$ is a continuous function whose value is contained within the region of $[0, 1]$.

The degree matrix $D(G)$ of graph G is defined as $D(G) = \text{diag}\{\sum_{j=1}^{N}(a_{ij}^1 + a_{ij}^2), i \in [1, N]\}$. The Laplacian matrix of the graph G is written as $L(G) = D(G) - A(G)$. Based on $A = A_1 + A_2$, we have $D(G) = D_1 + D_2$ and $L(G) = L_1 + L_2$, where $D_k = \text{diag}\{\sum_{j=1}^{N} a_{ij}^k, i \in [1, N]\}$ and $L_k = D_k - A_k$ represent the degree matrix and Laplacian matrix of graph G_k, respectively. Graph G_k is considered to be strongly connected if there always exists a directed path from a given node r_i to any other nodes in G_k. Graph G_1 is assumed to be static and strongly connected in this design. The following lemma is helpful for our future design of the sliding mode controller.

Lemma 2 ([10]): Consider the strongly connected digraph G_1, the matrix $(L_1 + B)$ is an irreducible nonsingular M-matrix if the matrix B is a nonnegative diagonal matrix with at least one positive entry. If we define

$$q = [q_1 \ q_2, \dots, q_N]^{\mathrm{T}} = (L_1 + B)^{-1} 1_{N\times 1}$$

then we get that $P_1 = \text{diag}\{\bar{p}_i\} = \text{diag}\{1/q_i\}$ is a positive definite matrix. Then, the matrix Q_1 defined as the following equation is symmetric and positive definite:

$$Q_1 = P_1(L_1 + B) + (L_1 + B)^{\mathrm{T}} P_1.$$

Assumption 3: Matrix L_2 and its time derivative $\dot{L}_2$ are bounded such that $\|L_2\|_F \le L_M^1$ and $\|\dot{L}_2\|_F \le L_M^2$.

Remark 1: The static communication graph G_1 is constructed to ensure that the overall topology G remains strongly connected, which further guarantees the robustness of the formation tracking process. Instead of relying on static communication topology, such as [9], the distance-related communication topology G_2 is defined so that each agent can obtain necessary information of nearby agents to avoid potential collisions.

C. RBFNN

Based on the idea of linearization, neural networks are usually employed to estimate the value of unknown or complex functions. In this article, the RBFNN [22] is implemented in the state observer to approximate uncertain function w_i

$$w_i = W_i^{\mathrm{T}} \varphi(y_i) + \epsilon_i \tag{6}$$

where $y_i \in \mathbb{R}^{m_1}$ is the input vector of the RBFNN of the ith agent, $W_i \in \mathbb{R}^{m\times n}$ is the optimal weight, ϵ_i is the network bias, and $\varphi(y_i) = [\varphi_1(y_i), \varphi_2(y_i), \dots, \varphi_m(y_i)]^{\mathrm{T}} \in \mathbb{R}^m$ is the Gaussian activation function that is given as

$$\varphi_j(y_i) = \exp\left[\frac{-(y_i - d_j)^{\mathrm{T}}(y_i - d_j)}{\mu^2}\right], \quad j = 1, 2, \dots, m \tag{7}$$

where $d_j = [d_{j,1}, d_{j,2}, \dots, d_{j,m_1}]^{\mathrm{T}}$ is the center of receptive field and μ denotes the width of the Gaussian function.

The estimation procedure of the RBFNN is given as

$$\widehat{w}_i = \widehat{W}_i^{\mathrm{T}} \varphi(y_i)$$

where $\widehat{W}_i \in \mathbb{R}^{m\times n}$ is the estimated weight matrix. The following lemma of RBFNNs is important for our later design.

Lemma 3 ([22]): When the approximated function w_i is bounded, the estimation error ϵ_i is expected to be bounded by a positive constant ϵ_M such that $\|\epsilon_i\| \le \epsilon_M$ is satisfied.

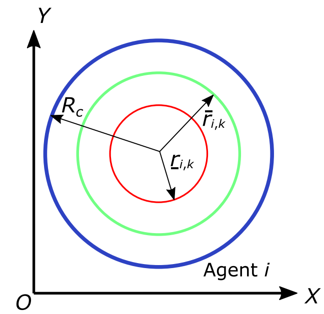

Fig. 1. Communication and APF ranges of agent i.

D. APF

In this article, APFs are implemented for all agents so that they can avoid colliding with each other. It is first assumed that the ith agent can be illustrated by a circle centered at x_{pi} with the radius of r_{ai}.

Now, we are ready to define the repulsive potential function $\Phi(\|z_{i,j}\|)$ between the ith and jth agents as follows:

Definition 2 ([9]): $\Phi(\|z_{i,j}\|)$ is a nonnegative, differentiable, and monotonically decreasing function that satisfies the following.

1) $\Phi(\|z_{i,j}\|) \to +\infty$ when $\|z_{i,j}\| \to \underline{r}_{i,j}$, where $\underline{r}_{i,j} = \epsilon_1(r_{a,i} + r_{a,j})$ is the minimal safe distance between the pair $\{i, j\}$, and ϵ_1 is a constant that satisfies $\epsilon_1 > 1$.
2) $\Phi(\|z_{i,j}\|) \to 0$ when $\|z_{i,j}\| \to \overline{r}_{i,j}$, and $\Phi(\|z_{i,j}\|) = 0$ when $\|z_{i,j}\| \ge \overline{r}_{i,j}$, where $\overline{r}_{i,j} = \epsilon_2(r_{a,i} + r_{a,j})$ represents the outer boundary of the APF, and ϵ_2 is a constant that satisfies $\overline{r}_{i,j} \in (\underline{r}_{i,j}, R_c]$ and $\overline{r}_{i,j} < \|x_{di} - x_{dj}\|$.

Based on the above discussion, the relationship between the APF and the limited range communication is given in Fig. 1.

The repulsive force generated between the ith and jth agents is obtained as the negative gradient of $\Phi(\|z_{i,j}\|)$, and the repulsive force posed on the ith agent is obtained as

$$f_{i,j} = -\nabla_{z_{i,j}} \Phi(\|z_{i,j}\|).$$

Then, we have the combined repulsive force f_i applied to the ith agent as

$$f_i = \sum_{j\in N_i} f_{i,j} = -\sum_{j\in N_i} \nabla_{z_{i,j}} \Phi(\|z_{i,j}\|)$$

where N_i is the neighbor set of the agent i in graph G.

In this article, the potential function is chosen as follows:

$$\Phi(\|z_{i,j}\|) = \begin{cases} \alpha \ln\left(\dfrac{\|z_{i,j}\| - \underline{r}_{i,j}}{\overline{r}_{i,j} - \underline{r}_{i,j}}\right) + \alpha \dfrac{\overline{r}_{i,j} - \|z_{i,j}\|}{\|z_{i,j}\| - \underline{r}_{i,j}}, & \text{for } \|z_{i,j}\| \in (\underline{r}_{i,j}, \overline{r}_{i,j}] \\ 0, & \text{otherwise.} \end{cases} \tag{8}$$

Accordingly, the repulsive force is obtained as

$$f_{i,j} = \begin{cases} \alpha \dfrac{\overline{r}_{i,j} - \|z_{i,j}\|}{(\|z_{i,j}\| - \underline{r}_{i,j})^2} \dfrac{z_{i,j}}{\|z_{i,j}\|}, & \text{for } \|z_{i,j}\| \in (\underline{r}_{i,j}, \overline{r}_{i,j}] \\ 0, & \text{otherwise.} \end{cases} \tag{9}$$

Remark 2: The outer boundary of the APF is chosen as $\overline{r}_{i,j} \le R_c$ to ensure that necessary position information is already obtained for each agent before generating the repulsive force f_i. The purpose of applying condition $\overline{r}_{i,j} < \|x_{di} - x_{dj}\|$ is that no redundant repulsive force is generated to disturb the system formation.

III. MAIN RESULTS

The main results of this article consist of two parts: designs and analysis of the finite-time neural-based state observer are presented in Section III-A, while the robust limited-information-based sliding mode controller is illustrated in Section III-B.

A. Finite-Time Neural-Based State Observer

Motivated by the neural-based observer designed in [18] and [23], we propose a finite-time neural-based state observer that can estimate both unknown system state and disturbance for agents with second-order dynamics (2) as follows:

$$\begin{aligned}\dot{\widehat{x}}_i &= \widehat{\upsilon}_i + \alpha_1 \mathrm{sgn}^{\beta_1}(x_i - \widehat{x}_i)\\ \dot{\widehat{\upsilon}}_i &= \alpha_2 \mathrm{sgn}^{\beta_2}(x_i - \widehat{x}_i) + g_i u_i + \widehat{W}_i^{\mathrm{T}} \varphi(y_i)\end{aligned} \tag{10}$$

where $\widehat{x}_i \in \mathbb{R}^n$ is the estimated position information, $\widehat{\upsilon}_i \in \mathbb{R}^n$ is the estimated velocity information, $y_i = [x_i^{\mathrm{T}}, \widehat{\upsilon}_i^{\mathrm{T}}]^{\mathrm{T}}$, $\alpha_1, \alpha_2 \in \mathbb{R}^+$, and $\beta_2 = 2\beta_1 - 1 > 0$. According to the approximating properties of RBFNNs, we have the expression of the estimation error as

$$\widetilde{\omega}_i = W_i^{\mathrm{T}}\varphi(y_i) + \epsilon_i - \widehat{W}_i^{\mathrm{T}}\varphi(y_i) = \widetilde{W}_i^{\mathrm{T}}\varphi(y_i) + \epsilon_i \tag{11}$$

where $\widetilde{W}_i = W_i - \widehat{W}_i$ denotes the weight estimation error.

With $\widetilde{x}_i = x_i - \widehat{x}_i$ and $\widetilde{\upsilon}_i = \upsilon_i - \widehat{\upsilon}_i$, we obtain the error dynamics of the neural-based observer as follows:

$$\begin{aligned}\dot{\widetilde{x}}_i &= \widetilde{\upsilon}_i - \alpha_1 \mathrm{sgn}^{\beta_1}(\widetilde{x}_i)\\ \dot{\widetilde{\upsilon}}_i &= \widetilde{\omega}_i - \alpha_2 \mathrm{sgn}^{\beta_2}(\widetilde{x}_i).\end{aligned} \tag{12}$$

Define $\bar{Z}_i = [\mathrm{sgn}^{\beta_1}(\widetilde{x}_i^{\mathrm{T}}), \widetilde{\upsilon}_i^{\mathrm{T}}]^{\mathrm{T}}$; then, we are able to obtain the time derivative of $\bar{Z}_i$ as

$$\begin{aligned}\dot{\bar{Z}}_i &= \begin{bmatrix}\beta_1 \mathrm{diag}\big(|\widetilde{x}_i|^{\beta_1 - 1}\big)\big(-\alpha_1 \mathrm{sgn}^{\beta_1}(\widetilde{x}_i) + \widetilde{\upsilon}_i\big)\\ -\alpha_2 \mathrm{sgn}^{\beta_2}(\widetilde{x}_i)\end{bmatrix} + \begin{bmatrix}0\\ \widetilde{\omega}_i\end{bmatrix}\\ &= \mathcal{Z}_i \mathcal{A}\bar{Z}_i + \mathcal{B}\widetilde{\omega}_i\end{aligned}$$

where the following equations are applied:

$$\begin{aligned}\mathcal{Z}_i &= \mathrm{diag}\Big(\Big[\big|\widetilde{x}_i^{\mathrm{T}}\big|^{\beta_1 - 1}, \big|\widetilde{x}_i^{\mathrm{T}}\big|^{\beta_1 - 1}\Big]\Big)\\ \mathcal{A} &= \begin{bmatrix}-\alpha_1\beta_1 I_n & \beta_1 I_n\\ -\alpha_2 I_n & 0_{n\times n}\end{bmatrix}, \quad \mathcal{B} = \begin{bmatrix}0_{n\times n}\\ I_n\end{bmatrix}.\end{aligned}$$

To ensure the boundedness of the observation error, the online weight tuning law of the RBFNN is chosen as follows:

$$\dot{\widehat{W}}_i = \gamma_1 \varphi(y_i)\mathrm{sgn}^{\beta_1}\big(\widetilde{x}_i^{\mathrm{T}}\big) - \gamma_2 \big\|\mathrm{sgn}^{\beta_1}\big(\widetilde{x}_i^{\mathrm{T}}\big)\big\| \widehat{W}_i. \tag{13}$$

The following lemmas are helpful for the stability analysis of the neural-based observer.

Lemma 4 ([24]): If $\mathcal{A}$ is a Hurwitz matrix, there always exists a symmetric positive definite matrix P_2 such that

$$\mathcal{A}^{\mathrm{T}} P_2 + P_2 \mathcal{A} = -Q_2$$

where Q_2 is a symmetric positive definite matrix.

Lemma 5 ([17]): Consider a positive definite Lyapunov candidate $V(\widetilde{x}_i, \widetilde{\upsilon}_i, \widetilde{W}_i)$ for a nonlinear agent (2); if its time derivative satisfies the condition that

$$\dot{V} \le -\bar{\beta}_1 V^{\bar{\alpha}_1} + \bar{\beta}_2 V^{\bar{\alpha}_2}$$

where $0 < \bar{\alpha}_2 < \bar{\alpha}_1 < 1$ and $\bar{\beta}_1, \bar{\beta}_2 > 0$, then the error states $\widetilde{x}_i$, $\widetilde{\upsilon}_i$, and $\widetilde{W}_i$ are all finite-time UUB. The function $V(\widetilde{x}_i, \widetilde{\upsilon}_i, \widetilde{W}_i)$ is contained within the attraction region of

$$\Omega_V = \left\{\left(\widetilde{x}_i, \widetilde{\upsilon}_i, \widetilde{W}_i\right) \,\middle|\, V\left(\widetilde{x}_i, \widetilde{\upsilon}_i, \widetilde{W}_i\right) \le \sqrt[\bar{\alpha}_1 - \bar{\alpha}_2]{\bar{\beta}_2/\bar{\beta}_3}\right\}$$

where $\bar{\beta}_3 \in (0, \bar{\beta}_1)$. Define t_0 as the initial time; then, the boundary of the settling time is obtained as

$$T \le V^{1-\bar{\alpha}_2}(t_0)/\big[\big(\bar{\beta}_1 - \bar{\beta}_3\big)(1 - \bar{\alpha}_1)\big].$$

Theorem 1: Consider the ith nonlinear agent (2), suppose that Assumption 1 holds, the update law of the RBFNN is chosen as (13), and the parameters are chosen reasonably within the constrains of $\alpha_1, \alpha_2 > 0$, $0.5 < \beta_1 < 1$, and $\beta_2 = 2\beta_1 - 1$; then, the neural-based observer (10) can guarantee that $\widetilde{W}_i$ is UUB and $\bar{Z}_i$ is finite-time UUB.

Proof: The characteristic polynomial of $\mathcal{A}$ is obtained as

$$\det(\lambda I_2 - \mathcal{A}) = \lambda^2 + \alpha_1\beta_1\lambda + \alpha_2\beta_1$$

which indicates that $\mathcal{A}$ is a Hurwitz matrix.

We define a Lyapunov candidate V_o as follows:

$$V_o = \frac{1}{2}\bar{Z}_i^{\mathrm{T}} P_2 \bar{Z}_i + \frac{1}{2}\mathrm{tr}\big\{\widetilde{W}_i^{\mathrm{T}}\widetilde{W}_i\big\}. \tag{14}$$

By Lemma 4, if we define $\mathcal{C} = [I_n, 0_{n\times n}]$, we are able to obtain the time derivative of V_o as follows:

$$\begin{aligned}\dot{V}_o &= -\frac{1}{2}\bar{Z}_i^{\mathrm{T}}\mathcal{Z}_i Q_2 \bar{Z}_i - \bar{Z}_i^{\mathrm{T}} P_2 \mathcal{B}\widetilde{\omega}_i - \mathrm{tr}\Big\{\widetilde{W}_i^{\mathrm{T}}\dot{\widehat{W}}_i\Big\}\\ &= -\frac{1}{2}\bar{Z}_i^{\mathrm{T}}\mathcal{Z}_i Q_2 \bar{Z}_i - \bar{Z}_i^{\mathrm{T}} P_2 \mathcal{B}\big(\widetilde{W}_i^{\mathrm{T}}\varphi(y_i) + \epsilon_i\big) + \gamma_1 \cdot\\ &\qquad \mathrm{tr}\Big\{\widetilde{W}_i^{\mathrm{T}}\varphi(y_i)\big(\mathcal{C}\bar{Z}_i\big)^{\mathrm{T}}\Big\} + \gamma_2 \mathrm{tr}\big\{\widetilde{W}_i^{\mathrm{T}}\|\mathcal{C}\bar{Z}_i\|\big(W_i - \widetilde{W}_i\big)\big\}.\end{aligned} \tag{15}$$

By Lemma 3, if we apply the inequalities $\|W_i\|_F \le W_M$, $\mathrm{tr}\{\widetilde{W}_i(W_i - \widetilde{W}_i)\} \le W_M\|\widetilde{W}_i\|_F - \|\widetilde{W}_i\|_F^2$, and $\varphi(y_i) \le \varphi_M$, we can rewrite (15) into the following equations:

$$\begin{aligned}\dot{V}_o \le -\frac{1}{2}\underline{\sigma}(Q_2)\|\bar{Z}_i\|^{3-1/\beta_1} + \big(k_3 + k_2\|\widetilde{W}_i\|_F\big)\|\bar{Z}_i\|\\ - \gamma_2 k_1 \|\bar{Z}_i\|\|\widetilde{W}_i\|_F^2\end{aligned} \tag{16}$$

where $k_1 = \|\mathcal{C}\|$, $k_2 = \varphi_M \max(|\overline{\sigma}(\mathcal{P}_1)|, |\underline{\sigma}(\mathcal{P}_1)|) + \gamma_2 k_1 W_M$, $\mathcal{P}_1 = P_2\mathcal{B} + \gamma_1\mathcal{C}$, and $k_3 = \overline{\sigma}(P_2)\epsilon_M$. Then, we have

$$\begin{aligned}\dot{V}_o &\le -\frac{1}{2}\underline{\sigma}(Q_2)\|\bar{Z}_i\|^{3-1/\beta_1}\\ &\quad + \left(-k_1\gamma_2\left(\|\widetilde{W}_i\|_F - \frac{k_2}{2k_1\gamma_2}\right)^2 + k_3 + \frac{k_2^2}{4k_1\gamma_2}\right)\|\bar{Z}_i\|\\ &\le -\frac{1}{2}\underline{\sigma}(Q_2)\|\bar{Z}_i\|^{3-1/\beta_1} + \left(k_3 + \frac{k_2^2}{4k_1\gamma_2}\right)\|\bar{Z}_i\|.\end{aligned}$$

Therefore, the negativeness of function $\dot{V}_o$ is guaranteed within the following region:

$$\Omega_z = \Big\{\|\bar{Z}_i\| \Big| \|\bar{Z}_i\| > \bar{\mathcal{K}}\Big\} \tag{17}$$

where $\bar{\mathcal{K}} = ((4k_1k_3\gamma_2 + k_2^2)/(2k_1\gamma_2\underline{\sigma}(Q_2)))^{2-1/\beta_1}$. By Lemma 1, the boundedness of the observation error is proven. Similarly, the weight estimation error $\widetilde{W}$ is also UUB according to a standard Lyapunov theory extension mentioned in [25].

Consider another function V_z as follows:

$$V_z = \frac{1}{2}\bar{Z}_i^{\mathrm{T}} P_2 \bar{Z}_i. \tag{18}$$

If we have $\|\widetilde{W}\|_F \le \widetilde{W}_M$, we can then obtain

$$\begin{aligned}\dot{V}_z &= \frac{1}{2}\bar{Z}_i^{\mathrm{T}}\mathcal{Z}_i\left(\mathcal{A}^{\mathrm{T}}P_2 + P_2\mathcal{A}\right)\bar{Z}_i - \bar{Z}_i^{\mathrm{T}}P_2\mathcal{B}\widetilde{\omega}_i \\ &= -\frac{1}{2}\bar{Z}_i^{\mathrm{T}}\mathcal{Z}_i Q_2\bar{Z}_i - \bar{Z}_i^{\mathrm{T}}P_2\mathcal{B}\left(\widetilde{W}_i^{\mathrm{T}}\varphi(y_i) + \epsilon_i\right) \\ &\le -\frac{1}{2}\underline{\sigma}(Q_2)\|\bar{Z}_i\|^{3-1/\beta_1} + k_4\|\bar{Z}_i\|\end{aligned} \tag{19}$$

where $k_4 = \overline{\sigma}(P_2)\epsilon_M + \overline{\sigma}(P_2\mathcal{B})\widetilde{W}_M\varphi_M$. By the inequality that $\underline{\sigma}(P_2)\|\bar{Z}_i\|^2/2 \le V_z \le \overline{\sigma}(P_2)\|\bar{Z}_i\|^2/2$, we have

$$\dot{V}_z \le -k_5 V_z^{(3\beta_1-1)/2\beta_1} + k_6 V_z^{1/2} \tag{20}$$

where equations $k_5 = (\overline{\sigma}(P_2)/2)^{(1-3\beta_1)/2\beta_1}\underline{\sigma}(Q_2)/2$ and $k_6 = k_4(2/\underline{\sigma}(P_2))^{1/2}$ are applied.

By Lemma 5, the error vector $\bar{Z}_i$ of the proposed observer (10) is finite-time UUB, which completes the proof. $\square$

Notice that inequality (16) used in the proof of Theorem 1 can be rewritten as follows:

$$\begin{aligned}\dot{V}_o &\le -\frac{1}{2}\underline{\sigma}(Q_2)\|\bar{Z}_i\|^{1-1/\beta_1}\|\bar{Z}_i\|^2 + k_2\|\widetilde{W}_i\|_F\|\bar{Z}_i\| \\ &\quad + k_3\|\bar{Z}_i\| - \gamma_2\|\bar{Z}_i\|\|\widetilde{W}_i\|_F^2 \\ &\le -\chi^{\mathrm{T}}H\chi + \mathcal{H}\chi\end{aligned} \tag{21}$$

where

$$\chi = \begin{bmatrix}\|\bar{Z}_i\| \\ \|\widetilde{W}_i\|_F\end{bmatrix}, \quad \mathcal{H} = \begin{bmatrix}k_3 & 0\end{bmatrix}$$
$$H = \begin{bmatrix}\underline{\sigma}(Q_2)\|\bar{Z}_i\|^{1-1/\beta_1}/2 & -k_2/2 \\ -k_2/2 & \gamma_2\|\bar{Z}_i\|\end{bmatrix}.$$

It is observed in (21) that the positiveness of H is determined by the value of $\det(H) = \underline{\sigma}(Q_2)\gamma_2\|\bar{Z}_i\|^{2-1/\beta_1}/2 - k_2^2/4$. Theoretically, we need to offer high values to γ_1 and γ_2 so that the matrix H is positive definite to further guarantee the convergence of $\bar{Z}_i$.

However, high values of γ_1 and γ_2 will also introduce high error-sensitivity in (13) and lead to oscillations or even instability when the value of $\|\bar{Z}_i\|$ is too high. Therefore, the performance of the observer is unsatisfactory if we only have static weight tuning parameters. Hence, a new varying-parameter neural-based observer is further introduced.

Because the vector $\bar{Z}_i$ is not completely known to the agent, it is necessary to find a substitute for it. According to our previous design of the neural network tuning law in (13), we can treat the parameters γ_1 and γ_2 as the amplifiers of the value of $\|\mathrm{sgn}^{\beta_1}(\widetilde{z}_1)\|$. Hence, it is reasonable to choose the value of $\|\mathrm{sgn}^{\beta_1}(\widetilde{z}_1)\|$ as the criteria to set the values of γ_1 and γ_2. For analyzing, after slicing the value region of $\|\mathrm{sgn}^{\beta_1}(\widetilde{z}_1)\|$ exponentially into n_υ ($n_\upsilon \in \mathbb{R}^+$) parts, we define the value sets $\bar{\gamma}_1$ and $\bar{\gamma}_2$ as follows:

$$\bar{\gamma}_i = \left[\bar{\gamma}_{i,1}, \bar{\gamma}_{i,2}, \ldots, \bar{\gamma}_{i,n_\upsilon}\right], \quad i = 1, 2.$$

By defining a constant $c_\upsilon \in \mathbb{R}$, we present the fractional parameter design as

$$\gamma_i = \begin{cases}\bar{\gamma}_{i,1}, & \|\mathrm{sgn}^{\beta_1}(\widetilde{z}_1)\| \in \left[10^{c_\upsilon-1}, +\infty\right) \\ \bar{\gamma}_{i,2}, & \|\mathrm{sgn}^{\beta_1}(\widetilde{z}_1)\| \in \left[10^{c_\upsilon-2}, 10^{c_\upsilon-1}\right) \\ \vdots, & \vdots \\ \bar{\gamma}_{i,j}, & \|\mathrm{sgn}^{\beta_1}(\widetilde{z}_1)\| \in \left[10^{c_\upsilon-j}, 10^{c_\upsilon-j+1}\right) \\ \vdots, & \vdots \\ \bar{\gamma}_{i,n_\upsilon}, & \|\mathrm{sgn}^{\beta_1}(\widetilde{z}_1)\| \in \left[0, 10^{c_\upsilon-n_\upsilon+1}\right)\end{cases} \tag{22}$$

where $j = 1, 2, \ldots, n_\upsilon$.

Theorem 2: Consider a second-order agent (2), and Assumption 1 holds. By the RBFNN update law (13) and the neural-based observer (10), it is guaranteed that the weight estimation error $\widetilde{W}_i$ is UUB, and the estimation error $\bar{Z}_i$ is finite-time UUB if the parameters of the observer are chosen reasonably within the constrains of $\alpha_1, \alpha_2 > 0$, $0.5 < \beta_1 < 1$ and $\beta_2 = 2\beta_1 - 1$, and the sets $\bar{\gamma}_1$ and $\bar{\gamma}_2$ are chosen properly within the following region:

$$\Omega_{\bar{\gamma}} = \begin{cases}\left\{\left(\bar{\gamma}_{1,j}, \bar{\gamma}_{2,j}\right)\middle|\bar{\mathcal{K}} < 10^{c_\upsilon-j}\right\}, & j \in [1, n_\upsilon) \\ \left\{\left(\bar{\gamma}_{1,j}, \bar{\gamma}_{2,j}\right)\middle|\bar{\mathcal{K}} < 10^{c_\upsilon-n_\upsilon+1}\right\}, & j = n_\upsilon.\end{cases} \tag{23}$$

Proof: According to (17), if we have $\gamma_1 = \bar{\gamma}_{1,j}$ and $\gamma_2 = \bar{\gamma}_{2,j}$ when $j \in [1, n_\upsilon - 1]$, we have

$$\sqrt[2-1/\beta_1]{\frac{4k_1k_3\gamma_2 + k_2^2}{2k_1\gamma_2\underline{\sigma}(Q_2)}} < 10^{c_\upsilon-j}$$

which indicates that $\|\bar{Z}_i\|$ will further converge to the $(j+1)$th fractional region mentioned in (22).

Otherwise, for $j = n_\upsilon$, we have $\gamma_1 = \bar{\gamma}_{1,n_\upsilon}$ and $\gamma_2 = \bar{\gamma}_{2,n_\upsilon}$ that further lead to

$$\sqrt[2-1/\beta_1]{\frac{4k_1k_3\gamma_2 + k_2^2}{2k_1\gamma_2\underline{\sigma}(Q_2)}} < 10^{c_\upsilon-n_\upsilon+1}.$$

We can then guarantee that $\|\bar{Z}_i\|$ is restricted within the n_υth fractional region, which leads to the uniform ultimate boundedness of both $\|\bar{Z}_i\|$ and $\|\widetilde{W}_i\|_F$. The proof of the finite-time characteristic of $\|\bar{Z}_i\|$ is similar to the one of Theorem 1. Hence, the proof is completed. $\square$

Remark 3: We choose the RBFNN because its Gaussian activation function can ensure the boundedness of vector $\varphi(y_i)$ regardless of the value of our estimation $\widehat{\upsilon}_i$, which further decreases the chance of having oscillations in its output. Theoretically, the finite-time neural-based observer design can also be extended to fit higher order systems.

B. Robust Sliding Mode Controller With Limited Information

For a second-order heterogeneous multiagent system (3), the position and velocity tracking errors of the ith agent are

$$\begin{cases}\delta_{xi} = x_i - x_{di} \\ \delta_{\upsilon i} = \upsilon_i - \dot{x}_{di}.\end{cases} \tag{24}$$

The error dynamics of the cluster are expressed as

$$\begin{cases} \dot{\delta}_x = \delta_v \\ \dot{\delta}_v = -\ddot{x}_d + gu + w \end{cases} \tag{25}$$

where $\delta_x = [\delta_{x1}^{\mathrm{T}}, \delta_{x2}^{\mathrm{T}}, \ldots, \delta_{xN}^{\mathrm{T}}]^{\mathrm{T}}$, $\delta_v = [\delta_{v1}^{\mathrm{T}}, \delta_{v2}^{\mathrm{T}}, \ldots, \delta_{vN}^{\mathrm{T}}]^{\mathrm{T}}$, and $x_d = [x_{d1}^{\mathrm{T}}, x_{d2}^{\mathrm{T}}, \ldots, x_{dN}^{\mathrm{T}}]^{\mathrm{T}}$.

With $e_{xi} \in \mathbb{R}^n$ and $e_{vi} \in \mathbb{R}^n$ being the local formation and velocity tracking error, respectively, we obtain

$$\begin{cases} e_{xi} = \sum_{j=1}^{N} a_{ij}\left(\delta_{xi} - \delta_{xj}\right) + b_i\delta_{xi} = \sum_{j=1}^{N} l_{ij}\delta_{xj} + b_i\delta_{xi} \\ e_{vi} = \sum_{j=1}^{N} a_{ij}\left(\delta_{vi} - \delta_{vj}\right) + b_i\delta_{vi} = \sum_{j=1}^{N} l_{ij}\delta_{vj} + b_i\delta_{vi} \end{cases} \tag{26}$$

where b_i is the ith diagonal element of matrix B.

Define the sliding variable s_i for agent i as

$$s_i = e_{vi} + \lambda_i e_{xi} \tag{27}$$

where λ_i is a positive constant.

Then, the sliding vector for the cluster is expressed as

$$\begin{aligned} S &= e_v + \Lambda \otimes I_n e_x \\ &= (L + B) \otimes I_n(\delta_v + \Lambda \otimes I_n\delta_x) \end{aligned} \tag{28}$$

where the following terms are applied:

$$\begin{aligned} e_x &= \left[e_{x1}^{\mathrm{T}}, e_{x2}^{\mathrm{T}}, \ldots, e_{xN}^{\mathrm{T}}\right]^{\mathrm{T}}, \quad e_v = \left[e_{v1}^{\mathrm{T}}, e_{v2}^{\mathrm{T}}, \ldots, e_{vN}^{\mathrm{T}}\right]^{\mathrm{T}} \\ S &= \left[s_1^{\mathrm{T}}, s_2^{\mathrm{T}}, \ldots, s_N^{\mathrm{T}}\right]^{\mathrm{T}}, \quad \Lambda = \mathrm{diag}\{\lambda_1, \lambda_2, \ldots, \lambda_N\}. \end{aligned}$$

In order to estimate the first- and second-order derivatives of the position reference x_{di}, a four-layer sliding mode differentiator [26] is employed for each agent

$$\begin{cases} \dot{\xi}_{i,1} = \nu_{i,1},\ \dot{\xi}_{i,2} = \nu_{i,2},\ \dot{\xi}_{i,3} = \nu_{i,3},\ \dot{\xi}_{i,4} = \nu_{i,4} \\ \nu_{i,1} = -\eta_{i,1}\beta_{i,x}^{\frac{1}{4}}\mathrm{sgn}^{\frac{3}{4}}\left(\xi_{i,1} - x_{di}\right) + \xi_{i,2} \\ \nu_{i,2} = -\eta_{i,2}\beta_{i,x}^{\frac{1}{3}}\mathrm{sgn}^{\frac{2}{3}}\left(\xi_{i,2} - \nu_{i,1}\right) + \xi_{i,3} \\ \nu_{i,3} = -\eta_{i,3}\beta_{i,x}^{\frac{1}{2}}\mathrm{sgn}^{\frac{1}{2}}\left(\xi_{i,3} - \nu_{i,2}\right) + \xi_{i,4} \\ \nu_{i,4} = -\eta_{i,4}\beta_{i,x}\mathrm{sgn}\left(\xi_{i,4} - \nu_{i,3}\right) \end{cases} \tag{29}$$

where $\widehat{x}_{di}^{(j-1)} = \xi_{i,j}$ $(j = 1, 2, 3, 4)$ stands for the estimation of the $(j-1)$th time derivative of x_{di}. With the implementation of the finite-time neural-based observer (10), we have the approximated velocity tracking error, local velocity tracking error, and sliding variable as

$$\widehat{\delta}_{vi} = \widehat{v}_i - \xi_{i,2},\ \widehat{e}_{vi} = \sum_{j=1}^{N} l_{ij}\widehat{\delta}_{vj} + b_i\widehat{\delta}_{vi},\ \widehat{s}_i = \widehat{e}_{vi} + \lambda_i e_{xi}. \tag{30}$$

Then, the estimated sliding vector for the entire system is written as

$$\begin{aligned} \widehat{S} &= \widehat{e}_v + \Lambda \otimes I_n e_x \\ &= (L + B) \otimes I_n\left(\widehat{\delta}_v + \Lambda \otimes I_n\delta_x\right). \end{aligned} \tag{31}$$

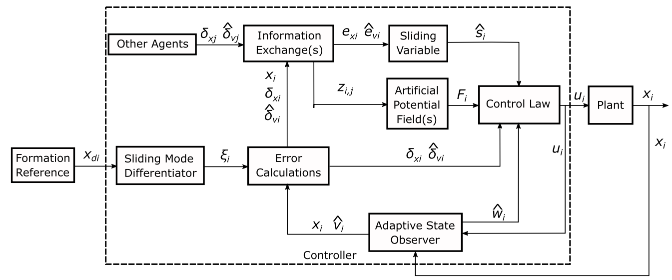

Fig. 2. Limited-information-based controller design.

According to (28), we have the time derivative as follows:

$$\dot{S} = (L + B) \otimes I_n(-\ddot{x}_d + gu + w + \Lambda \otimes I_n\delta_v) + \dot{L}_2 \otimes I_n (\delta_v + \Lambda \otimes I_n\delta_x). \tag{32}$$

Based on the discussions about the APF (9), the neural-based observer (10), the sliding mode differentiator (29), and the limited-information-based sliding variable (30), we are ready to present the limited-information-based formation controller design for the ith agent as

$$u_i = g_i^{-1}\left(-c\widehat{s}_i - \widehat{w}_i - \lambda_i\widehat{\delta}_{vi} - \delta_{xi} + \xi_{i,3} + F_i\right) \tag{33}$$

where $F_i = [f_i^{\mathrm{T}}, 0_{1\times n_2}]^{\mathrm{T}}$ and $c \in \mathbb{R}^+$. Based on the above discussions, our system design is illustrated in Fig. 2.

The following lemma is helpful for the stability proof of the limited information-based controller design:

Lemma 6 ([26]): With the parameters properly chosen for the sliding mode differentiator (29), if there is no input noise regarding the implemented differentiator, the following equations are true for agent i within a finite-time t_d:

$$\xi_{i,j} = x_{di}^{(j-1)},\ i = 1, 2, \ldots, n, \quad j = 1, 2, 3, 4.$$

Now, we are ready to present our controller design.

Theorem 3: Consider a second-order multiagent system (3) with limited information that satisfies Assumptions 1–3; by the implementation of finite-time neural-based observer (10), sliding mode differentiator (29) and APF between pairs of agents (8), the uniform ultimate boundedness of the sliding variable S, the local formation tracking error e_x, and the position tracking error δ_x can all be assured if we employ the limited-information-based sliding mode controller (33) with the parameters that satisfy conditions $c\underline{\sigma}(Q_1)/2 - \overline{\sigma}(P_1)L_M^2/\underline{\sigma}(L_1 + B) > 0$ and $\underline{\sigma}(\Lambda) - L_M^2/\underline{\sigma}(L_1 + B) > 0$.

Proof: This is a two-parted proof, where the effectiveness of the collision avoidance scheme and the formation controller is proved, respectively.

Part 1: In this part, we offer analysis regarding the proposed collision avoidance mechanism. For simplicity, the proof of collision is conducted on the agent pair $\{i, j\}$, where $i, j \in [1, N]$ and $i \neq j$. The same result can also be extended to any other agent pair.

Consider an energy-based Lyapunov function as follows:

$$V_{\mathrm{col}} = \frac{1}{2}z_{i,j}^{\mathrm{T}}z_{i,j} + \frac{1}{2}v_i^{\mathrm{T}}v_i + \frac{1}{2}v_j^{\mathrm{T}}v_j. \tag{34}$$

Accordingly, we have its time derivative as

$$\dot{V}_{\rm col} = z_{i,j}^{\rm T}\left(\upsilon_{pi} - \upsilon_{pj}\right) + \sum_{k=i,j} \upsilon_k^{\rm T}\left(-c\widehat{s}_k + \widetilde{w}_k - \lambda_k\widehat{\delta}_{\upsilon k} - \delta_{xk} + \xi_{k,3}\right) + \sum_{k=i,j} \upsilon_{pk}^{\rm T} f_k. \quad (35)$$

By Assumptions 1 and 2, terms $\sum_{k=i,j} \upsilon_k^{\rm T}(-c\widehat{s}_k + \widetilde{w}_k - \lambda_k\widehat{\delta}_{\upsilon k} - \delta_{xk} + \xi_{k,3})$ and $z_{i,j}^{\rm T}(\upsilon_{pi} - \upsilon_{pj})$ should be bounded in any time. For the scenario where the ith agent is running toward the jth agent, with the condition that $\sum_{k=i,j} \upsilon_{pk}^{\rm T} f_k \to +\infty$ when $\|z_{i,j}\| \to \underline{r}_{i,j}$, we always have $\dot{V}_{\rm col} \to +\infty$ when $\|z_{i,j}\|$ is small enough. Such a result will further lead to a boost of $\|z_{i,j}\|$ that indicates the separation of the agent pair $\{i, j\}$.

Meanwhile, we obtain the following equation based on the condition that $\|x_{di} - x_{dj}\| > \overline{r}_{i,j}$:

$$\lim_{t\to+\infty} \|F_i\| = 0, \quad i = 1, 2, \ldots, N. \quad (36)$$

Part 2: To prove the uniform ultimate boundedness of the sliding variable S and local formation tracking error e_x, we construct the following Lyapunov function:

$$V_F = \frac{1}{2}S^{\rm T} P_1 \otimes I_n S + \frac{1}{2}e_x^{\rm T} P_1 \otimes I_n e_x. \quad (37)$$

Similar to [27], the time derivative of V_F is obtained as

$$\begin{aligned}\dot{V}_F =\ & S^{\rm T}(P_1(L+B)) \otimes I_n\big(-\ddot{x}_d - c\widehat{S} - \widetilde{w} - \delta_x + \xi_3 + F \\ & + \Lambda \otimes I_n\big(\delta_\upsilon - \widehat{\delta}_\upsilon\big)\big) \\ & + e_x^{\rm T} P_1 \otimes I_n S - e_x^{\rm T}(P_1\Lambda) \otimes I_n e_x \\ & + S^{\rm T}\big(P_1\dot{L}_2\big) \otimes I_n(\delta_\upsilon + \Lambda \otimes I_n\delta_x) + e_x^{\rm T}\big(P_1\dot{L}_2\big) \otimes I_n\delta_x. \end{aligned} \quad (38)$$

Define $\widetilde{\xi}_3 = \xi_3 - \ddot{x}_d$, $\widetilde{\xi}_2 = \xi_2 - \dot{x}_d$, $\widetilde{\upsilon} = \widehat{\upsilon} - \upsilon$, $\widetilde{w} = \widehat{w} - w$, $\widehat{\upsilon} = [\widehat{\upsilon}_1^{\rm T}, \widehat{\upsilon}_2^{\rm T}, \ldots, \widehat{\upsilon}_N^{\rm T}]^{\rm T}$, and $\widehat{w} = [\widehat{w}_1^{\rm T}, \widehat{w}_2^{\rm T}, \ldots, \widehat{w}_N^{\rm T}]^{\rm T}$. By Lemma 6, we get that both $\widetilde{\xi}_2$ and $\widetilde{\xi}_3$ will converge to 0 after finite-time t_d. By Lemma 2, we further obtain

$$\begin{aligned}&\dot{V}_F \\ &= S^{\rm T}(P_1(L+B)) \otimes I_n(F - \widetilde{w} - cS - c(L+B) \otimes I_n\widetilde{\upsilon} \\ &\quad - \Lambda \otimes I_n\widetilde{\upsilon}) + S^{\rm T}\big(P_1\dot{L}_2(L+B)^{-1}\big) \otimes I_n S - e_x^{\rm T}(P_1\Lambda) \\ &\quad \otimes I_n e_x + e_x^{\rm T}\big(P_1\dot{L}_2(L+B)^{-1}\big) \otimes I_n e_x \\ &\le (\mathcal{K}_3(\widetilde{w}_M + \|F\|) + \mathcal{K}_4\widetilde{\upsilon}_M)\|S\| - \mathcal{K}_2\|S\|^2 - \mathcal{K}_5\|e_x\|^2 \\ &\le -\begin{bmatrix}\|S\| & \|e_x\|\end{bmatrix}\begin{bmatrix}\mathcal{K}_2 & 0 \\ 0 & \mathcal{K}_5\end{bmatrix}\begin{bmatrix}\|S\| \\ \|e_x\|\end{bmatrix} + \begin{bmatrix}\mathcal{K}_6 & 0\end{bmatrix}\begin{bmatrix}\|S\| \\ \|e_x\|\end{bmatrix}\end{aligned} \quad (39)$$

where $\mathcal{K}_1 = \overline{\sigma}(L+B)$, $\mathcal{K}_2 = c\underline{\sigma}(Q_1)/2 - \overline{\sigma}(P_1)L_M^2/\underline{\sigma}(L_1+B)$, $\mathcal{K}_3 = (\overline{\sigma}(P_1)L_M^1 + \overline{\sigma}(Q_1)/2)$, $\mathcal{K}_4 = \overline{\sigma}(P_1)\mathcal{K}_1(\overline{\sigma}(\Lambda) + c\mathcal{K}_1)$, $\mathcal{K}_5 = \underline{\sigma}(P_1)(\underline{\sigma}(\Lambda) - L_M^2/\underline{\sigma}(L_1+B))$, $\mathcal{K}_6 = \mathcal{K}_3(\widetilde{w}_M + \|F\|) + \mathcal{K}_4\widetilde{\upsilon}_M$, $\|\widetilde{w}\| \le \widetilde{w}_M$, and $\|\widetilde{\upsilon}\| \le \widetilde{\upsilon}_M$ are applied.

By the inequality $\underline{\sigma}(L+B) \ge \underline{\sigma}(L_1+B)$, we have the following inequality when $\|F\| = 0$:

$$\|S\| \le \frac{\mathcal{K}_7}{\min(\mathcal{K}_2, \mathcal{K}_5)}, \quad \|e_x\| \le \frac{\mathcal{K}_7}{\min(\mathcal{K}_2, \mathcal{K}_5)}$$
$$\|\delta_x\| \le \frac{\mathcal{K}_7}{\underline{\sigma}(L_1+B)\min(\mathcal{K}_2, \mathcal{K}_5)} \quad (40)$$

where $\mathcal{K}_7 = \mathcal{K}_3\widetilde{w}_M + \mathcal{K}_4\widetilde{\upsilon}_M$. Particularly, if the formation reference satisfies $\min_{(i,j)}\|x_{di} - x_{dj}\| > R_c$, we have the distance-based communication that satisfies

$$\lim_{t\to\infty}\big(||L_2(t)|| + ||\dot{L}_2(t)||\big) = 0.$$

Then, (40) has the alternative form of

$$\begin{aligned}\|S\| &\le \frac{\overline{\sigma}(Q_1)(\widetilde{w}_M + (c\overline{\sigma}(L_1+B) + \overline{\sigma}(\Lambda))\widetilde{\upsilon}_M)}{\min\big(c\underline{\sigma}(Q_1), 2\underline{\sigma}(Q_1)\underline{\sigma}(\Lambda)\big)} \\ \|e_x\| &\le \frac{\overline{\sigma}(Q_1)(\widetilde{w}_M + (c\overline{\sigma}(L_1+B) + \overline{\sigma}(\Lambda))\widetilde{\upsilon}_M)}{\min\big(c\underline{\sigma}(Q_1), 2\underline{\sigma}(Q_1)\underline{\sigma}(\Lambda)\big)} \\ \|\delta_x\| &\le \frac{\overline{\sigma}(Q_1)(\widetilde{w}_M + (c\overline{\sigma}(L_1+B) + \overline{\sigma}(\Lambda))\widetilde{\upsilon}_M)}{\underline{\sigma}(L_1+B)\min\big(c\underline{\sigma}(Q_1), 2\underline{\sigma}(Q_1)\underline{\sigma}(\Lambda)\big)}\end{aligned} \quad (41)$$

which proves that S, e_x, and δ_x are UUB. □

Remark 4: According to (40) and (41), the convergence boundaries of the system states can be reduced if we properly increase the value of c and λ_i. Therefore, the upper limits of the convergence neighborhood can be manually designed regardless of each agent's initial states.

IV. Simulation and Results

To justify the performance of our proposed neural-based observer and the limited-information-based sliding mode controller, numerical simulations based on a multiple omnidirectional robot system are conducted.

Consider a cluster of three-wheel omnidirectional robots [13], where the dynamics of agent i is written as

$$\begin{cases}\dot{x}_i = \upsilon_i \\ \dot{\upsilon}_i = M_i T_i u_i + w_i\end{cases} \quad (42)$$

where $x_i = [p_{xi}, p_{yi}, \theta_i]^{\rm T}$, $M_i = {\rm diag}\{1/m_i, 1/m_i, 1/I_i\}$, m_i is the mass of the robot, I_i is the inertia of the robot, $u_i = [F_{1i}, F_{2i}, F_{3i}]^{\rm T}$ is the force vector of the three motors, and T_i is a transformation matrix that can be written as

$$T_i = \begin{bmatrix}-\sin(\theta_{\rm i}) & -\sin(\pi/3 - \theta_{\rm i}) & \sin(\pi/3 + \theta_{\rm i}) \\ \cos(\theta_{\rm i}) & -\cos(\pi/3 - \theta_{\rm i}) & -\cos(\pi/3 + \theta_{\rm i}) \\ R_i & R_i & R_i\end{bmatrix}$$

where R_i is the radius of the robot. The dynamics related parameters and initial position are chosen, as shown in Table I. L_1 is selected as in Fig. 3 and $b_i = 2$ for $i \in [1, 6]$.

TABLE I
Parameters and Initial States

Robot number	Model parameters			Initial states		
	m(kg)	R(m)	$I(\mathrm{kg}\cdot\mathrm{m}^2)$	p_x(m)	p_y(m)	θ(rad)
1	4.8	0.24	0.15	1.8	0.1	0
2	5.5	0.30	0.25	-0.9	0.6	$\pi/3$
3	4.5	0.23	0.12	-0.7	2.3	$-\pi/3$
4	5.8	0.31	0.29	0.8	-0.5	$\pi/2$
5	5.3	0.28	0.21	-0.1	-1.3	$\pi/4$
6	5.0	0.25	0.15	1.5	1.5	$-\pi/4$

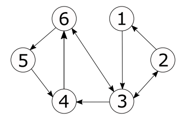

Fig. 3. Communication topology L_1.

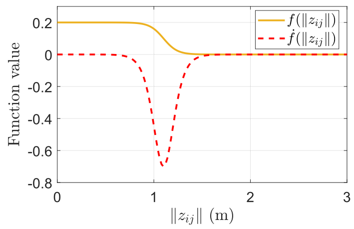

Fig. 4. Example of $f(\|z_{ij}\|)$ and its time derivative.

The position reference for the ith agent is chosen as

$$x_{di} = [1.8\cos(i\pi/3) + 0.2t, 1.8\sin(i\pi/3) + \sin(0.3t), 0]^{\mathrm{T}}. \tag{43}$$

The time-varying communication function $f(\|z_{ij}\|)$ for the distance-related communication is chosen in the form of

$$f\left(\|z_{ij}\|\right) = \begin{cases} \eta_1 \dfrac{e^{-\eta_2\left(\|z_{ij}\|-\eta_3\right)}}{1+e^{-\eta_2\left(\|z_{ij}\|-\eta_3\right)}}, & \|z_{ij}\| \in [0, R_c] \\ 0, & \|z_{ij}\| \in (R_c, +\infty) \end{cases} \tag{44}$$

where the parameter values are set as $\eta_1 = 0.2$, $\eta_2 = 14$, $\eta_3 = 1.1$, and $R_c = 1.5$ m. The values of $f(\|z_{ij}\|)$ and its time derivative $\dot{f}(\|z_{ij}\|)$ are illustrated in Fig. 4. The APF for each agent is constructed with the value selection of $\alpha = 2$, $\epsilon_1 = 1.1$, and $\epsilon_2 = 2$.

The parameters of the sliding mode differentiator are set as $\eta_{i,1} = \eta_{i,4} = 6$ and $\eta_{i,2} = \eta_{i,3} = 8$. By Theorem 3, the parameters of the sliding mode controller are set as $\lambda_i = 2$ and $c = 2$ for each agent. The uncertainty w_i is chosen as

$$\begin{aligned} w_i = [&0.5\sin(p_{xi}) + \tanh(p_{xi}) + 0.6\sin(0.6t + i\pi/5) \\ &0.3\sin\left(p_{yi}\right) - 1.4e^{-|p_{yi}|-1} + 0.8\sin(0.4t + i\pi/5) \\ &0.2\cos(\theta_i) + \sin(0.5t + i\pi/5)]^{\mathrm{T}}. \end{aligned}$$

First, we define the following three error norms to justify our designs of the finite-time neural-based observer:

$$\mathcal{N}_x = \sum_{i=1}^{6} \|\widetilde{x}_i\|, \quad \mathcal{N}_v = \sum_{i=1}^{6} \|\widetilde{v}_i\|, \quad \mathcal{N}_w = \sum_{i=1}^{6} \|\widetilde{w}_i\|.$$

By Theorem 1, the basic parameters for the observers are chosen as $\beta_1 = 2/3$, $\alpha_1 = 8$, and $\alpha_2 = 8$. For RBFNNs, the number of neurons is chosen as $m = 8$, the receptive field centers are chosen as $d_j = (j-3)\mathbf{1}_{2n} (j \in [1, m])$, and the width of the Gaussian function is set as $\mu = 8$. Here, we choose the following three designs for the performance comparison regarding the values of $\mathcal{N}_x$, $\mathcal{N}_v$, and $\mathcal{N}_w$.

1) The original finite-time observer (OFTO) in [24] is

$$\begin{aligned} \dot{\widehat{x}}_i &= \widehat{v}_i - \alpha_1 \mathrm{sgn}^{\beta_1}(\widetilde{x}_i) \\ \dot{\widehat{v}}_i &= \widehat{w}_i - \alpha_2 \mathrm{sgn}^{\beta_2}(\widetilde{x}_i) + g_i u_i \\ \dot{\widehat{w}}_i &= -\alpha_3 \mathrm{sgn}^{\beta_2}(\widetilde{x}_i) \end{aligned} \tag{45}$$

with the parameter α_3 chosen as $\alpha_3 = 6$.

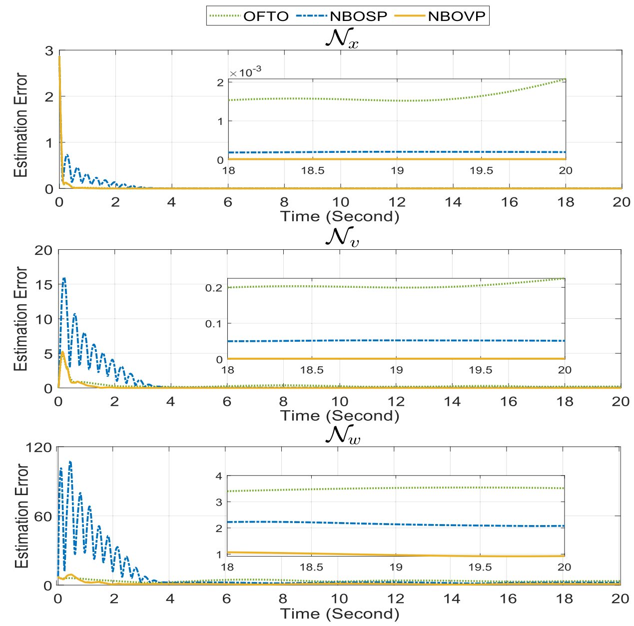

Fig. 5. Performance comparisons among three observers.

TABLE II

OBSERVER ACCURACY COMPARISONS

Criteria	Observer designs		
	OFTO	NBOSP	NBOVP
$\mathcal{N}_x$	4.2×10^{-3}	2.1×10^{-4}	1.5×10^{-5}
$\mathcal{N}_v$	2.3×10^{-1}	5.3×10^{-2}	1.7×10^{-3}
$\mathcal{N}_w$	4.1	2.3	1.1

2) The neural-based observer (10) with static parameters (NBOSP) where the weight tuning parameters in (13) are chosen as $\gamma_1 = 200$ and $\gamma_2 = 20$.

3) The neural-based observer (10) with varying parameters (NBOVP) where the weight tuning parameters in (13) are chosen as follows by Theorem 2:

$$\begin{aligned} \bar{\gamma}_1 &= [1, 5, 50, 200, 10000] \\ \bar{\gamma}_2 &= [0.05, 0.25, 5, 20, 100]. \end{aligned} \tag{46}$$

The comparative results of the observer designs are presented in Fig. 5, and the bounded regions of $\mathcal{N}_x$, $\mathcal{N}_v$, and $\mathcal{N}_w$ are provided in Table II. The finite-time observer designs proposed in this article are observed to have higher precision than the OFTO in [24]. The validity of Theorem 1 is proven by the results of NBOSP. NBOVP is observed to have a convergence time of 2.3 s, which is shorter than NBOSP (4 s). Moreover, the NBOVP design can also attenuate the oscillation of the RBFNN output and increase the estimation accuracy simultaneously, illustrating the validity of Theorem 2.

Since the NBOVP design is proven to have higher estimation accuracy, it is employed in all later comparative simulations, if not specially stated otherwise. To illustrate that the range-based communication topology G_2 is helpful for

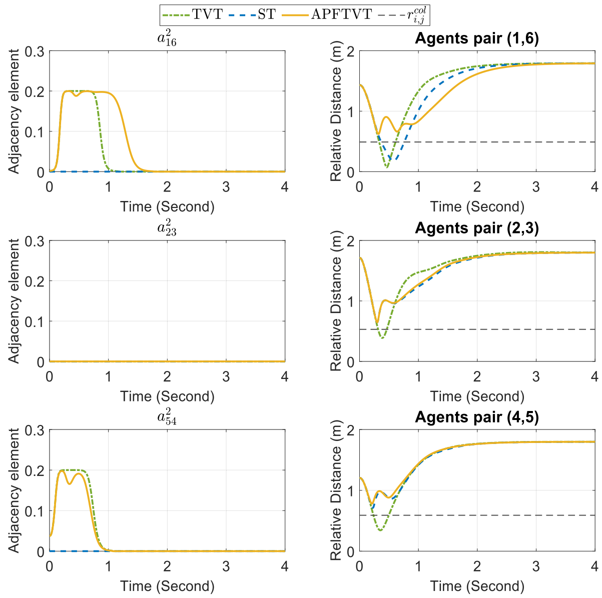

Fig. 6. Propagation of adjacency elements in A_2 and effectiveness of the collision avoidance scheme.

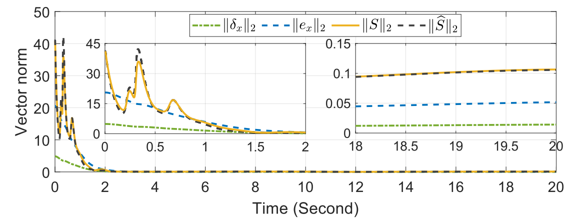

Fig. 7. Performance of the limited-information-based formation controller.

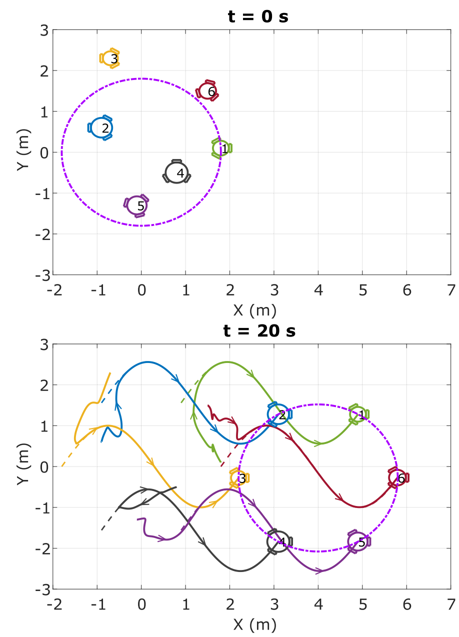

Fig. 8. Trajectories of the system.

avoiding potential collisions, we choose the following three scenarios where (30) is implemented.

1) The APF in (8) is implemented along with static topology (ST) that satisfies $L = L_1$.
2) The APF is disabled ($\|F_i\| = 0$), while we have the time-varying topology (TVT) that satisfies $L = L_1 + L_2$.
3) The APF is implemented along with the TVT (APFTVT) that satisfies $L = L_1 + L_2$.

By defining $r_{i,j}^{\text{col}} = R_i + R_j$ to be the relative distance of the agent pair $\{i, j\}$ when collision happens, we have the comparative results, as shown in Fig. 6. The result of TVT shows that these agents will collide if the APF is not implemented. Although the static graph G_1 is capable to ensure that the agent pairs with communication (pairs $\{2, 3\}$ and $\{4, 5\}$) are able to avoid a potential collision, the ST design is insufficient for those without direct communication, such as pair $\{1, 6\}$. The system can be considered as collision-free if and only if we employ both the APF and the range-based communication, indicating the necessity and effectiveness of having G_2. It is measured that the APFTVT method can guarantee inequalities $\|z_{i,j}\| > \underline{r}_{i,j}$ and $\|z_{i,j}\| \geq r_{i,j}^{\text{col}} + 0.1$ in this simulation. The propagation of three related elements in the adjacency matrix A_2 is also given in Fig. 6, where we observe that necessary edges (see a_{16}^2 and a_{54}^2) are formed when potential collision is expected, but no new edge is generated when the connection has already existed in the static graph G_1 (see a_{23}^2), which satisfies our design in (5).

The norms of system states are presented in Fig. 7, where we can see that $\|\delta_x\|_2$ is bounded within 0.016, $\|e_x\|_2$ is bounded within 0.057, and the values of $\|S\|_2$ and $\|\widehat{S}\|_2$ are bounded within 0.12 simultaneously. The trajectories of all agents are presented in Fig. 8 to better illustrate the movement and formation status of the entire system. According to (43), the formation reference is a circular formation whose center moves in a sine-wave trajectory (purple circle). It is observed that each agent follows its reference trajectory (dotted line) with bounded tracking error and composes the expected formation successfully, which illustrates the effectiveness of our proposed distributed formation controller (33).

Remark 5: For a formation tracking task where there is at least one channel of the agent's position state whose norm is expected to have a linear relationship with time, such as (43), we need to enlarge the width of the Gaussian function by increasing the value of μ. Otherwise, potential divergence issue will occur when t is large enough because $\varphi(y_i)$ will lose sensitivity to y_i if $\|y_i - d_j\|$ is too large.

V. Conclusion

In this article, the robust and collision-free formation control problem for second-order multiagent systems with limited information was investigated. A new finite-time neural-based state observer was first designed to estimate the unknown velocity and disturbance. Furthermore, an error-related observer parameter design was proposed to attenuate the chattering phenomenon and increase approximation precision. By introducing a distance-related directed topology, agents are able to obtain each other's position to generate repulsive force to avoid the collision. A distributed robust sliding mode control scheme was then proposed to ensure the uniform ultimate boundedness of the system's formation tracking error. The validity of each design is guaranteed by the Lyapunov stability theory and further illustrated by simulations and comparisons.

References

[1] R. Olfati-Saber and R. M. Murray, "Consensus problems in networks of agents with switching topology and time-delays," *IEEE Trans. Autom. Control*, vol. 49, no. 9, pp. 1520–1533, Sep. 2004.

[2] P. Shi and J. Yu, "Dissipativity-based consensus for fuzzy multiagent systems under switching directed topologies," *IEEE Trans. Fuzzy Syst.*, vol. 29, no. 5, pp. 1143–1151, May 2021.

[3] Q. Shen and P. Shi, "Distributed command filtered backstepping consensus tracking control of nonlinear multiple-agent systems in strict-feedback form," *Automatica*, vol. 53, pp. 120–124, Mar. 2015.

[4] C.-Y. Sun and C.-X. Mu, "Important scientific problems of multi-agent deep reinforcement learning," *Acta Autom. Sinica*, vol. 46, no. 7, pp. 1301–1312, 2020.

[5] J. Fei, K.-W. Chin, C. Yang, and M. Ros, "Charge-and-activate policies for targets monitoring in RF-harvesting sensor networks," *IEEE Trans. Veh. Technol.*, vol. 69, no. 7, pp. 7835–7846, Jul. 2020.

[6] X. Dong, Y. Hua, Y. Zhou, Z. Ren, and Y. Zhong, "Theory and experiment on formation-containment control of multiple multirotor unmanned aerial vehicle systems," *IEEE Trans. Autom. Sci. Eng.*, vol. 16, no. 1, pp. 229–240, Jan. 2019.

[7] Y. Liu, P. Shi, H. Yu, and C.-C. Lim, "Event-triggered probability-driven adaptive formation control for multiple elliptical agents," *IEEE Trans. Syst., Man, Cybern. Syst.*, early access, Oct. 16, 2020, doi: 10.1109/TSMC.2020.3026029.

[8] J. Yu, X. Dong, Q. Li, and Z. Ren, "Practical time-varying formation tracking for second-order nonlinear multiagent systems with multiple leaders using adaptive neural networks," *IEEE Trans. Neural Netw. Learn. Syst.*, vol. 29, no. 12, pp. 6015–6025, Dec. 2018.

[9] R. S. Sharma, A. Mondal, and L. Behera, "Tracking control of mobile robots in formation in the presence of disturbances," *IEEE Trans. Ind. Informat.*, vol. 17, no. 1, pp. 110–123, Jan. 2021.

[10] Y. Fei, P. Shi, and C.-C. Lim, "Robust formation control for multi-agent systems: A reference correction based approach," *IEEE Trans. Circuits Syst. I, Reg. Papers*, vol. 68, no. 6, pp. 2616–2625, Jun. 2021.

[11] M.-B. Radac and T. Lala, "Robust control of unknown observable nonlinear systems solved as a zero-sum game," *IEEE Access*, vol. 8, pp. 214153–214165, 2020.

[12] Z.-M. Li and X.-H. Chang, "Robust H_∞ control for networked control systems with randomly occurring uncertainties: Observer-based case," *ISA Trans.*, vol. 83, pp. 13–24, Dec. 2018.

[13] F. Yang, S. Peng, and C. C. Lim, "Neural network adaptive dynamic sliding mode formation control of multi-agent systems," *Int. J. Syst. Sci.*, vol. 51, no. 1, pp. 2025–2040, 2020.

[14] H. Lin, K. Chen, and R. Lin, "Finite-time formation control of unmanned vehicles using nonlinear sliding mode control with disturbances," *Int. J. Innov. Comput., Inf. Control*, vol. 15, no. 6, pp. 2341–2353, 2019.

[15] Y. Chu, J. Fei, and S. Hou, "Adaptive global sliding-mode control for dynamic systems using double hidden layer recurrent neural network structure," *IEEE Trans. Neural Netw. Learn. Syst.*, vol. 31, no. 4, pp. 1297–1309, Apr. 2020.

[16] J. Yu, X. Dong, Q. Li, and Z. Ren, "Practical time-varying formation tracking for high-order nonlinear multi-agent systems based on the distributed extended state observer," *Int. J. Control*, vol. 92, no. 10, pp. 2451–2462, Oct. 2019.

[17] Q. Hu and B. Jiang, "Continuous finite-time attitude control for rigid spacecraft based on angular velocity observer," *IEEE Trans. Aerosp. Electron. Syst.*, vol. 54, no. 3, pp. 1082–1092, Jun. 2018.

[18] Y. H. Kim, F. L. Lewis, and C. T. Abdallah, "A dynamic recurrent neural-network-based adaptive observer for a class of nonlinear systems," *Automatica*, vol. 33, no. 8, pp. 1539–1543, Aug. 1997.

[19] B. Chen, H. Zhang, X. Liu, and C. Lin, "Neural observer and adaptive neural control design for a class of nonlinear systems," *IEEE Trans. Neural Netw. Learn. Syst.*, vol. 29, no. 9, pp. 4261–4271, Sep. 2017.

[20] D. H. Lee, S. S. Lee, C. K. Ahn, P. Shi, and C.-C. Lim, "Finite distribution estimation-based dynamic window approach to reliable obstacle avoidance of mobile robot," *IEEE Trans. Ind. Electron.*, vol. 68, no. 10, pp. 9998–10006, Oct. 2021.

[21] S. Li and X. Wang, "Finite-time consensus and collision avoidance control algorithms for multiple AUVs," *Automatica*, vol. 49, no. 11, pp. 3359–3367, Nov. 2013.

[22] S. Zheng, P. Shi, S. Wang, and Y. Shi, "Adaptive neural control for a class of nonlinear multiagent systems," *IEEE Trans. Neural Netw. Learn. Syst.*, vol. 32, no. 2, pp. 763–776, Feb. 2021.

[23] D. Liu, Y. Huang, D. Wang, and Q. Wei, "Neural-network-observer-based optimal control for unknown nonlinear systems using adaptive dynamic programming," *Int. J. Control*, vol. 86, no. 9, pp. 1554–1566, Sep. 2013.

[24] B. Li, K. Qin, B. Xiao, and Y. Yang, "Finite-time extended state observer based fault tolerant output feedback control for attitude stabilization," *ISA Trans.*, vol. 91, pp. 11–20, Aug. 2019.

[25] Y. H. Kim and F. L. Lewis, "Neural network output feedback control of robot manipulators," *IEEE Trans. Robot. Autom.*, vol. 15, no. 2, pp. 301–309, Apr. 1999.

[26] A. Levant, "Higher-order sliding modes, differentiation and output-feedback control," *Int. J. Control*, vol. 76, nos. 9–10, pp. 924–941, Jan. 2003.

[27] J. Chen, J. Li, R. Zhang, and C. Wei, "Distributed fuzzy consensus of uncertain topology structure multi-agent systems with non-identical partially unknown control directions," *Appl. Math. Comput.*, vol. 362, Dec. 2019, Art. no. 124581.

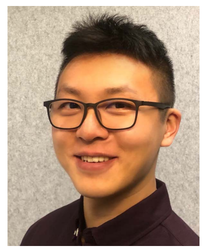

Yang Fei received the B.Eng. degree in automation from Harbin Institute of Technology, Heilongjiang, China, in 2018. He is currently pursuing the Ph.D. degree in electrical and electronic engineering with The University of Adelaide, Adelaide, SA, Australia.

His current research interests include multiagent systems, sliding mode control, and neural network adaptive control.

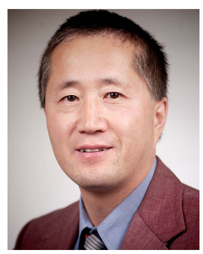

Peng Shi (Fellow, IEEE) received the Ph.D. degree in electrical engineering from The University of Newcastle, Callaghan, NSW, Australia, in 1994, the Ph.D. degree in mathematics from the University of South Australia, Adelaide, SA, Australia, in 1998, the D.Sc. degree from the University of Glamorgan, Pontypridd, U.K., in 2006, and the D.E. degree from The University of Adelaide, Adelaide, in 2015.

He is currently a Professor with The University of Adelaide. His research interests include systems and control theory and applications to autonomous and robotic systems, intelligence systems, network systems, and cyber–physical systems. He has published widely in these fields.

Dr. Shi is also a member of the Academy of Europe and a fellow of the Institution of Engineering and Technology (IET) and the Institute of Engineers, Australia (IEAust). He has been on the Editorial Board of a number of journals, including *Automatica*, IEEE Transactions on Automatic Control, IEEE Transactions on Cybernetics, IEEE Transactions on Fuzzy Systems, and IEEE Transactions on Circuits and Systems. He also serves as the President of the International Academy for Systems and Cybernetic Science and the Vice-President and a Distinguished Lecturer of the IEEE SMC Society.

Cheng-Chew Lim (Life Senior Member, IEEE) received the B.Sc. degree (Hons.) in electronic and electrical engineering and the Ph.D. degree in electronic and electrical engineering from Loughborough University, Leicestershire, U.K., in 1977 and 1981, respectively.

He is currently a Professor with The University of Adelaide, Adelaide, SA, Australia. His current research interests include control and system theory, autonomous systems, machine learning, and optimization techniques and applications.

Dr. Lim has served as an Associate Editor for the IEEE Transactions on Systems, Man, and Cybernetics: Systems, an Editorial Board Member of the *Journal of Industrial and Management Optimization*, and a Guest Editor for a number of journals, including *Discrete and Continuous Dynamical Systems-Series B*.